Eur. Phys. J. Special Topics **227**, 1969–1979 (2019)

https://doi.org/10.1140/epjst/e2018-800064-8

THE EUROPEAN PHYSICAL JOURNAL SPECIAL TOPICS

Regular Article

Thermoelectric transport through interacting quantum dots in graphene

José Ramón Isern-Lozano[1], Jong Soo Lim[3], Ioan Grosu[2], Rosa López[1], Mircea Crisan[2], and David Sánchez[1,a]

[1] Institute for Cross-Disciplinary Physics and Complex Systems IFISC (UIB-CSIC), 07122 Palma de Mallorca, Spain
[2] Department of Theoretical Physics, University of Cluj, 40084 Cluj-Napoca, Romania
[3] School of Physics, Korea Institute for Advanced Study, Seoul 130-722, Korea

Received 16 April 2018
Published online 24 January 2019

Abstract. We study the thermoelectric properties of an electronic localized level coupled to two graphene electrodes. Graphene band structure shows a pseudogap density of states (DOS) that strongly affects the charge transport. We focus on the Coulomb blockade regime and derive the expression for the Onsager matrix that relates the charge and heat currents to the voltage and temperature biases in the linear response regime. The elements of the Onsager matrix are functions of the transmission coefficient, which depends on the dot Green's function. Our self-consistent calculation of the Green's function is based on the equation-of-motion technique. We find a double-peak structure for the electric and thermal responses as the dot level is tuned with an external gate terminal, in accordance with the Coulomb blockade phenomenon. Remarkably enough, the thermal conductance is much smaller than its electric counterpart, giving rise to a high thermoelectric figure of merit for certain values of the gate voltage. Finally, we discuss a large departure from the Wiedemann–Franz law caused mainly by the pseudogap DOS in the contacts and weakly affected by interactions.

1 Introduction

Graphene, a monolayer of carbon atoms set on an hexagonal lattice, was firstly synthesized more than a decade ago [1,2]. The unusual properties of graphene are due to its Dirac-like band structure, where conduction and valence bands touch at six discrete points at the edges of the honeycomb Brillouin zone. The relativistic (Dirac) character of graphene electrons was pointed out by DiVincenzo and Mele [3] before graphene was grown in the lab. In its energy band structure, only two of the six Dirac cones are nonequivalent, being currently named as the K and K′ points [1]. The quasiparticle excitations at those points obey linear energy dispersions and are responsible for many exotic physical phenomena such as half-integer quantum Hall effect and Klein tunneling, among others [1]. Moreover, graphene quasiparticles are chiral fermions with potential applications in the so-called valleytronics field of research [4,5].

[a] e-mail: david.sanchez@uib.es

An appealing graphene application is found when graphene acts as a conductive material attached to a nanostructure to create a single-electron transistor. An example is the case of a quantum dot carved in a graphene sheet [6–9]. Here, typical Coulomb blockade phenomenon is observed associated to transport of charges across the localized dot level. The linear conductance exhibits peaks at the dot resonances separated by the mean-dot level spacing and electron–electron Coulomb repulsion. Interestingly, transport of charges in graphene-based quantum dots occur at much higher temperatures than in traditional semiconductor dots [9]. Further, under certain circumstances, many-body effects such as Kondo physics [10–12] could be observed. It has been shown that graphene alters quite strongly the Kondo state [13–22]. However, much less attention has received the Coulomb blockade regime in which charge fluctuations are the dominant events in transport. Coulomb-blockade effects are ubiquitous and govern the transport properties of a large variety of systems: quantum dots [23], molecular bridges [24], carbon nanotubes [25], etc. Coulomb blockade transport has been investigated extensively in nanostructures attached to metallic contacts. However, when contacts are graphene electrodes, the Coulomb blockade effect is a relatively unexplored problem. Experimentally, Coulomb blockade oscillations have been reported to occur in graphene quantum dots where the linear conductance oscillates with the dot level position [6,7].

Whereas a great deal of works has been devoted to the study of graphene electronic properties, the thermal and thermoelectric properties are less understood. Recent measurements reveal that graphene shows high thermal conductance values [26]. In this respect, graphene-based setups might offer novel opportunities to the progress in thermoelectrics [27–30]. Good thermoelectric devices at the nanoscale should be able to efficiently transform wasted heat into useful electricity or convert electric currents into reversible heat [31,32]. The figure of merit ZT is a coefficient that quantifies the efficiency in the heat-to-electricity (or electricity-to-heat) conversion process. Importantly, the figure of merit is proportional to the square of the Seebeck (thermopower) coefficient, namely, the ratio between the electric and thermoelectric linear conductances under open-circuit conditions.

The purpose of our work is to analyze the thermoelectric transport through an interacting quantum dot coupled to Dirac-like electrodes. We are interested in a temperature regime where charge fluctuations are important and therefore we neglect Kondo physics. Below, we develop a theoretical model that describes this system. We will consider the linear transport regime and compute electric ($\mathcal{G}$), thermal ($\mathcal{K}$), and thermoelectric responses $\mathcal{L}_{12}$. Our findings indicate that graphene single-electron transistors show rather high thermoelectric efficiencies with found values of $ZT \simeq 8$. As a byproduct, we demonstrate that due to the strong energy dependence of tunneling rates this system shows violations of the Wiedemann–Franz law.

The paper is organized as follows. In Section 2, we introduce our model for an interacting dot coupled to two Dirac contacts. The Onsager matrix is computed to describe electric and heat fluxes when voltage and temperature biases are applied, and the Seebeck and ZT coefficients are accordingly defined. Since transport coefficients depend on the dot Green's function, we apply an equation-of-motion (EOM) technique [33–36] to derive the conductances. Our results for different parameters are thoroughly discussed in Section 3. Finally, Section 4 summarizes the main achievements of this work.

2 Theoretical model

We employ an Anderson-like model to describe a spin degenerate localized level with strong on-site Coulomb interaction and coupled to two Dirac electrodes as shown in

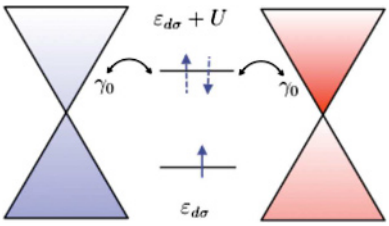

Fig. 1. Energy band diagram for the system under consideration. The dot level is denoted by $\varepsilon_{d\sigma}$. For double occupancy the dot level is shifted by an amount U that describes the Coulomb repulsion. The hybridization term $\Gamma(\varepsilon) = \gamma_0|\varepsilon - \mu|$ depends on energy ε. We consider undoped graphene electrodes with chemical potential $\mu = \varepsilon_F = 0$ located at the Dirac point. The electrodes can be held at different temperatures indicated by blue and red colors.

Figure 1. The full Hamiltonian reads [37,38]

$$\mathcal{H} = \sum_{\sigma} \varepsilon_{d\sigma} d^{\dagger}_{\sigma} d_{\sigma} + U n_{\uparrow} n_{\downarrow} + \sum_{\alpha=L/R,s,k,\sigma} \int_{-k_c}^{+k_c} dk (\varepsilon_k - \mu) c^{\dagger}_{\alpha s k \sigma} c_{\alpha s k \sigma}$$
$$+ \tilde{V} \sum_{i\,\sigma} \int_{-k_c}^{+k_c} dk \sqrt{|k|} \left(c^{\dagger}_{\alpha s k \sigma} d_{\sigma} + d^{\dagger}_{\sigma} c_{\alpha s k \sigma} \right), \tag{1}$$

where $d_\sigma(d^\dagger_\sigma)$ annihilates (creates) an electron with spin $\sigma = \{\uparrow, \downarrow\}$ in the localized level, $\varepsilon_{d\sigma}$ denotes the spin-resolved energy level, and U represents the strength of the Coulomb interaction. Here, $n_\sigma = d^\dagger_\sigma d_\sigma$ is the particle number operator for the localized level. In the graphene leads, $c_{\alpha sk\sigma}(c^\dagger_{\alpha sk\sigma})$ annihilates (creates) a relativistic electron in contact α ($= L/R$ for the left/right contact) with valley index s, wave vector k, and spin σ. The energy spectrum $\varepsilon_k = \hbar v_F k$ is relatively measured with respect to the chemical potential μ with $v_F \simeq 10^6$ m/s being the graphene Fermi velocity. The chemical potential μ can be tuned by doping techniques and, hereafter, we consider $\mu = \varepsilon_F = 0$. We recall that the linear dispersion $\varepsilon_k = \hbar v_F k$ leads to the linear density of states (DOS) $\rho(\varepsilon) \propto |\varepsilon|$. k_c is a momentum cutoff such that $D = \pm\hbar v_F k_c$ are the energy limits inside which the graphene continuum model is valid. Finally, the dot-lead coupling is $\tilde{V} = V_0\sqrt{\pi\Omega_0}/2\pi$, where Ω_0 is the area of the graphene unit cell and V_0 the tunneling amplitude.

2.1 Onsager matrix: transport coefficients

We now compute the transport coefficients expressed as the Onsager matrix [39] that connects linear charge and heat currents with the (small) applied forces, which in our case are the electrical and thermal biases:

$$\begin{pmatrix} \mathcal{I} \\ \mathcal{J} \end{pmatrix} = \begin{pmatrix} \mathcal{L}_{11} & \mathcal{L}_{12} \\ \mathcal{L}_{21} & \mathcal{L}_{22} \end{pmatrix} \begin{pmatrix} \Delta V \\ \Delta T \end{pmatrix}. \tag{2}$$

Here, $\mathcal{I}$ and $\mathcal{J}$ are the charge and heat currents, respectively, generated when an electric bias $\Delta V = V_L - V_R$ and a temperature difference $\Delta T = T_L - T_R$ are applied between the left and right contacts. In an explicit manner, the elements of the Onsager matrix are [40,41]

$$\mathcal{L}_{11} = \frac{e^2}{h}\int_{-\infty}^{+\infty} d\varepsilon\ \mathcal{T}(\varepsilon)\left[-\frac{\partial f(\varepsilon)}{\partial\varepsilon}\right]_{T,\mu}, \tag{3}$$

$$\mathcal{L}_{12} = \frac{e}{hT}\int_{-\infty}^{+\infty} d\varepsilon\ \mathcal{T}(\varepsilon)(\varepsilon-\mu)\left[-\frac{\partial f(\varepsilon)}{\partial\varepsilon}\right]_{T,\mu} = \mathcal{L}_{21}/T, \tag{4}$$

$$\mathcal{L}_{22} = \frac{1}{hT}\int_{-\infty}^{+\infty} d\varepsilon\ \mathcal{T}(\varepsilon)(\varepsilon-\mu)^2\left[-\frac{\partial f(\varepsilon)}{\partial\varepsilon}\right]_{T,\mu}, \tag{5}$$

where $\mathcal{T}(\varepsilon)$ is the transmission probability through the dot. The response coefficients ($\mathcal{L}_{ij}$) are now related to the linear electric $\mathcal{G} = \mathcal{L}_{11}$, thermal $\mathcal{K} = \mathcal{L}_{22} - T\frac{\mathcal{L}_{12}^2}{\mathcal{L}_{11}}$, and thermoelectric ($\mathcal{L}_{12}$) conductances. Since we focus on the linear response regime, all responses must be calculated at equilibrium. Hence, in the above expressions $f(\varepsilon) = 1/[\exp(\varepsilon/k_BT)+1]$ is the Fermi function at equilibrium with T the background temperature common to both graphene electrodes.

We define the Seebeck coefficient or themopower as

$$S = -\frac{\Delta V}{\Delta T}\Big|_{\mathcal{I}=0} = \frac{\mathcal{L}_{12}}{\mathcal{L}_{11}}. \tag{6}$$

This is useful for the calculation of the thermoelectric figure of merit:

$$ZT = \frac{S^2GT}{\mathcal{K}}. \tag{7}$$

An important remark here is in order. For sufficiently low temperatures the thermal conductance is dominated by purely electronic transport and therefore we can neglect the phonon contribution to ZT. We will later emphasize this point.

All transport coefficients are expressed in terms of the transmission coefficient

$$\mathcal{T}(\varepsilon) = 2\pi\Gamma(\varepsilon)\textstyle\sum_\sigma \rho_{d\sigma}(\varepsilon), \tag{8}$$

where $\Gamma(\varepsilon) = \gamma_0|\varepsilon|$ with $\gamma_0 = \pi\tilde{V}^2\rho_0$ (here, $\rho_0 = 2/(\hbar v_F)^2$). $\rho_{d\sigma}(\varepsilon)$ denotes the local DOS for the interacting level which can be found as $\rho_{d\sigma}(\varepsilon) = -\frac{1}{\pi}\Im\left(G^r_{\sigma,\sigma}(\varepsilon)\right)$. $G^r_{\sigma,\sigma}$ is the retarded Green function for the interacting localized level. In the following, we derive a Green's function suitable for the Coulomb blockade regime. To attain such a goal, we employ the EOM technique [34–36] followed by a decoupling procedure. We note that Kondo correlations are not included in our decoupling scheme.

2.2 Green's function

The retarded Green's function $G^r(t)$ for fermionic operators A and B is defined as

$$G^r_{A,B}(t) \equiv \langle\langle A, B\rangle\rangle^r_t = -i\theta(t)\langle\{A(t), B(0)\}\rangle, \tag{9}$$

whose EOM in energy space takes the following form

$$\varepsilon^+\langle\langle A, B\rangle\rangle^r_\varepsilon + \langle\langle[\mathcal{H}, A], B\rangle\rangle^r_\varepsilon = \langle\{A, B\}\rangle, \tag{10}$$

with $\mathcal{H}$ being the Hamiltonian under consideration and $\varepsilon^+ = \varepsilon + i0^+$. For the dot Green's function $G^r_{\sigma,\sigma}(\varepsilon) = \langle\langle d_\sigma, d^\dagger_\sigma \rangle\rangle^r_\varepsilon$, it is easy to show that

$$\left(\varepsilon^+ - \varepsilon_{d\sigma}\right) G^r_{\sigma,\sigma}(\varepsilon) = 1 + U \left\langle\left\langle d_\sigma n_{\bar\sigma}, d^\dagger_\sigma \right\rangle\right\rangle^r_\varepsilon + \widetilde{V} \sum_{\alpha,s} \int_{-k_c}^{k_c} dk \, \sqrt{|k|} \left\langle\left\langle c_{\alpha s k\sigma}, d^\dagger_\sigma \right\rangle\right\rangle^r_\varepsilon . \quad (11)$$

The equation for $\langle\langle c_{\alpha s k\sigma}, d^\dagger_\sigma \rangle\rangle^r_\varepsilon$ is found to be

$$\left\langle\left\langle c_{\alpha s k\sigma}, d^\dagger_\sigma \right\rangle\right\rangle^r_\varepsilon = \frac{\widetilde{V}\sqrt{|k|}}{\varepsilon^+ - \varepsilon_k} G^r_{\sigma,\sigma}(\varepsilon) \,, \quad (12)$$

such that the dot Green's function becomes

$$\left(\varepsilon - \varepsilon_{d\sigma} - \Sigma^r_0(\varepsilon)\right) G^r_{\sigma,\sigma}(\varepsilon) = 1 + U \left\langle\left\langle d_\sigma n_{\bar\sigma}, d^\dagger_\sigma \right\rangle\right\rangle^r_\varepsilon , \quad (13)$$

where $\Sigma^r_0(\varepsilon) = \widetilde{V}^2 \sum_{\alpha,s} \int_{-k_c}^{k_c} dk \, \frac{|k|}{\varepsilon^+ - \varepsilon_k}$ is the self-energy due to the hybridization between both graphene contacts and the localized level. The self-energy is evaluated as

$$\Sigma^r_0(\varepsilon) = -\eta \left[\varepsilon \ln \left| \frac{D^2 - \varepsilon^2}{\varepsilon^2} \right| + i\pi |\varepsilon| \Theta(D - |\varepsilon|) \right] , \quad (14)$$

where $\eta = 2(\tilde{V}/\hbar v_F)^2 = \gamma_0/\pi$.

In order to obtain the Coulomb blockade solution, we need to calculate the EOM for $\langle\langle d_\sigma n_{\bar\sigma}, d^\dagger_\sigma \rangle\rangle^r_\varepsilon$. This is given by

$$\begin{aligned}\left(\varepsilon^+ - \varepsilon_{d\sigma} - U\right) \left\langle\left\langle d_\sigma n_{\bar\sigma}, d^\dagger_\sigma \right\rangle\right\rangle^r_\varepsilon = \langle n_{\bar\sigma} \rangle + \widetilde{V} \textstyle\sum_{\alpha,s} \int_{-k_c}^{k_c} dk \, \sqrt{|k|} \left[\left\langle\left\langle c_{\alpha s k\sigma} n_{\bar\sigma}, d^\dagger_\sigma \right\rangle\right\rangle^r_\varepsilon \right. \\ \left. + \left\langle\left\langle d^\dagger_{\bar\sigma} c_{\alpha s k\bar\sigma} d_\sigma, d^\dagger_\sigma \right\rangle\right\rangle^r_\varepsilon - \left\langle\left\langle c^\dagger_{\alpha s k\bar\sigma} d_{\bar\sigma} d_\sigma, d^\dagger_\sigma \right\rangle\right\rangle^r_\varepsilon \right] . \quad (15)\end{aligned}$$

We keep only the correlation $\langle\langle c_{\alpha s k\sigma} n_{\bar\sigma}, d^\dagger_\sigma \rangle\rangle^r_\varepsilon$ on the right hand side and calculate its EOM, which can be approximated as

$$\left(\varepsilon^+ - \varepsilon_k\right) \left\langle\left\langle c_{\alpha s k\sigma} n_{\bar\sigma}, d^\dagger_\sigma \right\rangle\right\rangle^r_\varepsilon \approx \widetilde{V} \sqrt{|k|} \left\langle\left\langle d_\sigma n_{\bar\sigma}, d^\dagger_\sigma \right\rangle\right\rangle^r_\varepsilon . \quad (16)$$

After straightforward algebra, we obtain

$$G^r_{\sigma,\sigma}(\varepsilon) = \left[\frac{1 - \langle n_{\bar\sigma} \rangle}{\varepsilon - \varepsilon_{d\sigma} - \Sigma^r_0(\varepsilon)} + \frac{\langle n_{\bar\sigma} \rangle}{\varepsilon - \varepsilon_{d\sigma} - U - \Sigma^r_0(\varepsilon)} \right] . \quad (17)$$

The poles of $G^r_{\sigma,\sigma}(\varepsilon)$ are located around $\varepsilon_{d\sigma}$ and $\varepsilon_{d\sigma} + U$. As a consequence, this solution properly describes the Coulomb blockade regime. The dot occupation must be calculated self-consistently using

$$\langle n_\sigma \rangle = \int_{-D}^{+D} d\varepsilon \; f(\varepsilon) \left[-\frac{1}{\pi} \Im \left(G^r_{\sigma,\sigma}(\varepsilon) \right) \right] . \quad (18)$$

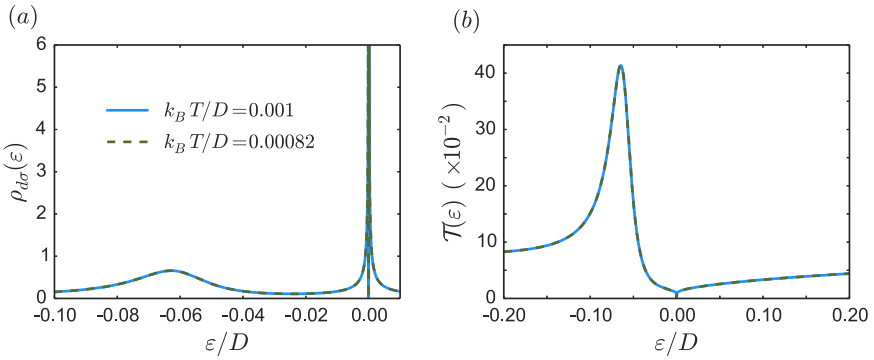

Fig. 2. (a) Dot density of states $\rho_{d\sigma}(\varepsilon)$ and (b) transmission coefficient $\mathcal{T}(\varepsilon)$ as a function of energy. We consider two distinct temperatures: $k_BT/D = 0.001$ (solid line) and 8.2×10^{-5} (dotted line). Parameters: $\varepsilon_{d\sigma} = -U$, $\eta = 0.1$, and $U/D = 0.1$.

3 Results

We now discuss our results for the transport properties of a graphene-based quantum dot with the aid of the model proposed above. Unless it is indicated, we consider the strong Coulomb blockade regime ($U = 0.1D$) and investigate how the transport properties depend on the dot level position, tuned with an externally applied gate electrode. Thus, we explore $\mathcal{G}$, $\mathcal{K}$, and the Seebeck and ZT coefficients.

In order to better understand the transport properties of our system, in Figure 2 we depict the behavior of the dot DOS and the transmission coefficient. It is shown that for $\varepsilon_{d\sigma} = -U$ the DOS displays two resonances located at $\varepsilon \approx \varepsilon_{d\sigma} + \Re e\Sigma_0(\varepsilon)$ and $\varepsilon \approx \varepsilon_{d\sigma} + U + \Re e\Sigma_0(\varepsilon)$. The resonance around the Fermi energy ($\varepsilon = 0$) is very narrow in comparison with the low-energy resonance at $\varepsilon \simeq -0.06$, which is broader. This is explained by the fact that the hybridization depends strongly on energy. In addition, the dot spectral function at the Fermi energy becomes maximum. Nevertheless, even if the local DOS reaches the highest value at ε_F, the transmission coefficient, evaluated at the Fermi energy, vanishes. This is illustrated in Figure 2b. The transmission coefficient is the product of the contact and dot DOSs. The former vanishes exactly at ε_F, giving rise to a vanishingly small transmission coefficient despite the fact that the dot DOS attains at $\varepsilon = 0$ its highest value. The fact that the transmission coefficient is zero at ε_F yields a two-dip structure for $\mathcal{G}$ as a function of the dot level position, as shown below.

We next discuss the electric and thermal conductances when the dot level is tuned. We start by showing the evolution of $\mathcal{G}$ as a function of the dot level for various values of the on-site interaction U (see Fig. 3). For the noninteracting case ($U/D = 0$), the conductance exhibits a dip (antiresonance) at the contact Fermi energy ε_F. In general, the antiresonance occurs when the localized level aligns with ε_F because the contact DOS vanishes at the charge neutrality point. In the presence of Coulomb interactions ($U > 0$), there are two effective levels lying at ε_d and $\varepsilon_d + U$. When these two levels align with ε_F, the transmission again vanishes due to the nonavailability of states of the graphene contacts at ε_F. The transmission shows a dip that resembles a Fano singularity originated from destructive interference. However, the origin of the dip in our setup is instead due to the lack of electronic states of the graphene contacts. Another worthy aspect of $\mathcal{G}$ is the fact that the peaks close to the dips are not symmetric. Around $\varepsilon_{d\sigma} = -U$, the two maxima differ in their heights. This results from the fact that the DOS of the quasilocalized level is not symmetric with respect to the resonance points.

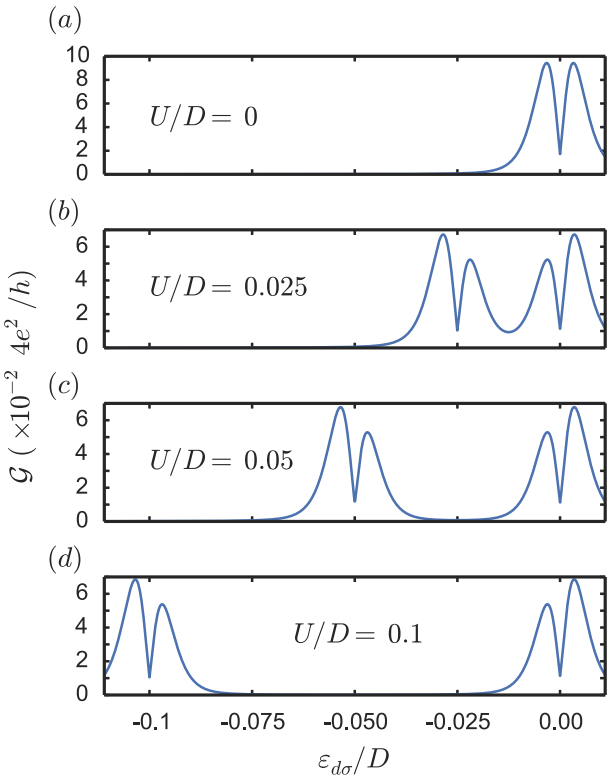

Fig. 3. Electric conductance $\mathcal{G}$ as a function of the dot level $\varepsilon_{d\sigma}$ for different values of the charging energy: $U/D = 0$ (a), 0.025 (b), 0.05 (c), and 0.1 (d). Parameters: $\eta = 0.1$ and $k_B T/D = 0.001$.

We focus on the strong interacting case where Coulomb blockade phenomenon is better exhibited and choose $U/D = 0.1$. Our purpose is to analyze the temperature dependence of the electric $\mathcal{G}$ and thermal $\mathcal{K}$ conductances as shown in Figure 4a and c, respectively. We observe that $\mathcal{G}$ has moderate temperature dependence as a function of the gate voltage. In the middle of the Coulomb valley, thermal activation is not sufficient to cause a quantitative change in $\mathcal{G}$. In stark contrast, $\mathcal{K}$ shows a more dramatic behavior as a function of $\varepsilon_{d\sigma}$. The first remarkable fact is the absence of the dips at the resonance points. Even though electric transport is suppressed at the resonance points, heat transport is mostly insensitive to the transmission dip.

Importantly, the thermal conductance is three orders of magnitude smaller than $\mathcal{G}$ when compared with their respective quanta. This is a noticeable feature inasmuch normal conductors typically possess high electric and thermal conductances simultaneously. Good thermoelectrical devices are those that display poor thermal conductances and high electric conductances just like our graphene single-electron transistor. In metallic conductors, the Wiedemann–Franz law

$$\frac{\mathcal{K}}{\mathcal{G}T} = \frac{\pi^2}{3}\left(\frac{k_B}{e}\right)^2, \tag{19}$$

is satisfied in a wide temperature range. By utilizing graphene contacts, such a relation between $\mathcal{G}$ and $\mathcal{K}$ is violated. Consequently, the Seebeck coefficient attains much higher values. This fact is precisely illustrated in Figure 4b, where the Seebeck

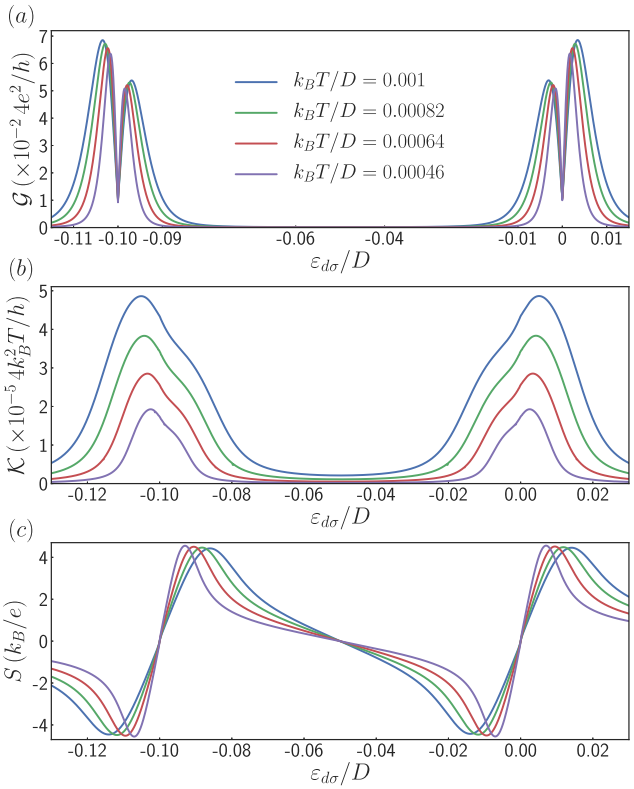

Fig. 4. (a) Electric conductance $\mathcal{G}$ and (b) thermal conductance $\mathcal{K}$ versus dot level $\varepsilon_{d\sigma}$ for various values of the temperature k_BT/D, and (c) Seebeck coefficient S versus $\varepsilon_{d\sigma}$ for various k_BT/D. Parameters: $\eta = 0.1$ and $U/D = 0.1$.

coefficient is displayed as a function of $\varepsilon_{d\sigma}$ for various background temperatures T. We find that the Seebeck coefficient reaches high values, $S \gtrsim 4$ in units of $k_B/e = 86\,\mu\text{V/K}$ [42]. As expected, S vanishes at the resonance points $\varepsilon_{d\sigma} = \varepsilon_F$ and $\varepsilon_{d\sigma} + U = \varepsilon_F$. Around these points, S is an odd function of $\varepsilon_{d\sigma}$. Related with S is the figure of merit ZT. In equation (7), the thermal conductance $\mathcal{K}$ contains the electronic and phonon contributions (i.e., $\mathcal{K} = \mathcal{K}_e + \mathcal{K}_{ph}$). Through this work, $\mathcal{K}_{ph}$ is neglected since we assume the low temperature case. Furthermore, in graphene the thermal conductance due to phonons can be tailored to very low values even at room temperature by employing anti-dots or nanoribbons [43]. Therefore, it is safe to neglect the phonon contribution in our calculations of the thermal conductance.

The reported large values of ZT indicate that heat-to-electricity conversion process is performed with high efficiency. Good thermoelectrical conductors can exhibit $ZT \gtrsim 1$. Our device shows ZT values close to 8 as illustrated in Figure 5b, which might have important consequences for practical applications. These results for the figure of merit ZT can be compared with those achieved for the case of a localized level tunnel coupled to normal contacts with an energy independent tunneling rate Γ. Such comparison is performed in Figure 5a, where the ZT values for the normal dot case are displayed. We observe that much smaller ZT values are reached and therefore the graphene leads play a crucial role in the generation of high ZT values.

In Figure 6, we investigate the Wiedemann–Franz law. As anticipated, the Wiedemann–Franz law is not fulfilled. To pinpoint the main source of such violation,

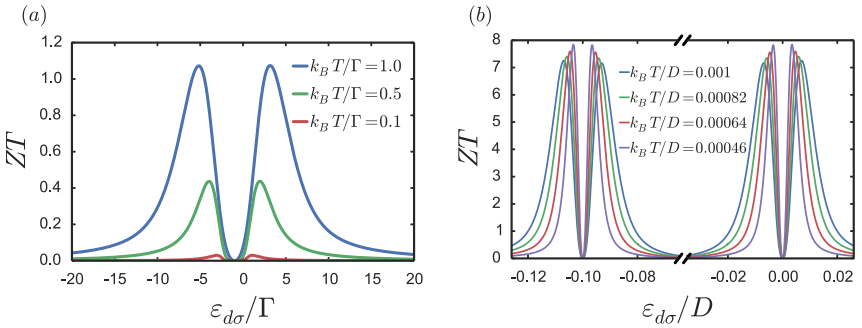

Fig. 5. Figure of merit ZT as a function of $\varepsilon_{d\sigma}$. Comparison between metallic contacts (a) when k_BT/Γ is changed and graphene contacts (b) when k_BT/D is changed. Parameters for metallic contacts: $D/\Gamma = 100$, and $U/\Gamma = 2$. Parameters for graphene contacts: $\eta = 0.1$, and $U/D = 0.1$.

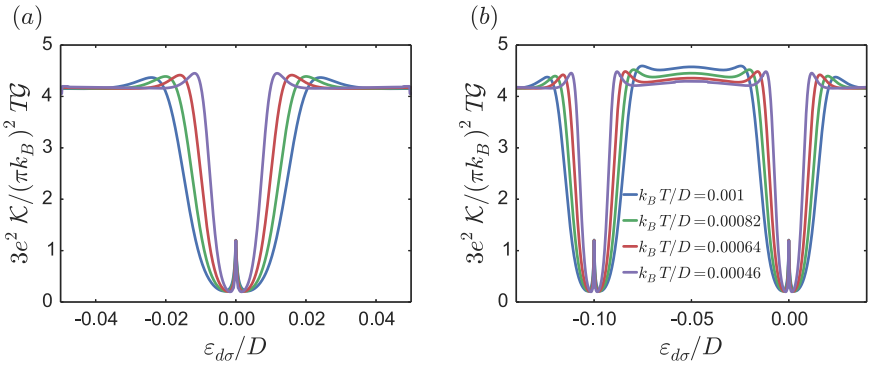

Fig. 6. Violation of the Wiedemann–Franz law as a function of $\varepsilon_{d\sigma}$ for $U/D = 0$ (noninteracting case), $\eta = 0.1$ (a) and $U/D = 0.1$ (interacting case), $\eta = 0.1$ (b). As shown, several temperatures are considered.

we consider $U = 0$ and $U > 0$ cases. We observe that the violation of the Wiedemann–Franz is not connected to electron–electron interactions [44] but instead is due to the Dirac-like energy dispersion relation of the contacts. We recall that equation (19) is based on a Sommerfeld expansion, which is valid for transmissions $\mathcal{T}(\varepsilon)$ weakly dependent on ε around the Fermi energy. This condition may hold for metallic leads with flat DOS but is broken in our system due to the pseudogap in graphene.

4 Conclusions

In closing, we have analyzed the linear electric, thermal, and thermoelectric linear responses for an interacting localized level coupled to Dirac-like electrodes as in graphene. Our results support the prospect that Dirac-like electrodes lead to more efficient thermoelectric devices with large values for both the Seebeck and ZT coefficients. The latter can reach values as high as $ZT \simeq 8$. Indeed, due to the strong energy dependence of the DOS at the electrodes our graphene-based device displays an anomalously low thermal conductance in contrast to the values reached for the electric conductance. These two facts yield high thermoelectric figures of merit. Moreover, such energy dependence is responsible for the violation of the Wiedemann–Franz

law. We believe that our reported values for the ZT in graphene coupled quantum dots will motivate their experimental verification using present technology (e.g., using graphene bilayer dots [45]). Future works should examine the role of strong correlations or larger electric and thermal biases [46].

This work was supported by MINECO Grant No. MAT2017-82639.

References

1. A.H.C. Neto, F. Guinea, N.M.R. Peres, K.S. Novoselov, A.K. Geim, Rev. Mod. Phys. **81**, 109 (2009)
2. A.K. Geim, K.S. Novoselov, Nat. Mater. **6**, 183 (2007)
3. D. DiVincenzo, E.J. Mele, Phys. Rev. B **29**, 1685 (1984)
4. C.E. Nebel, Nat. Mater. **12**, 690 (2013)
5. M.B. Lundeberg, J.A. Folk, Science **346**, 422 (2014)
6. C. Stampfer, J. Güttinger, F. Molitor, D. Graf, T. Ihn, K. Ensslin, Appl. Phys. Lett. **92**, 012102 (2008)
7. C. Stampfer, E. Schurtenberger, F. Molitor, J. Guettinger, T. Ihn, K. Ensslin, Nano Lett. **8**, 2378 (2008)
8. F. Sols, F. Guinea, A.H.C. Neto, Phys. Rev. Lett. **99**, 166803 (2007)
9. R. Murali, *Graphene Nanoelectronics: From Materials to Circuits* (Springer-Verlag, NY, 2012)
10. A.C. Hewson, *The Kondo Problem to Heavy Fermions* (Cambridge University Press, Cambridge, 1993)
11. S.M. Cronenwett, T.H. Oosterkamp, L.P. Kouwenhoven, Science **281**, 540 (1998)
12. D. Goldhaber-Gordon, H. Shtrikman, D. Mahalu, D. Abusch-Magder, U. Meirav, M.A. Kastner, Nature **391**, 156 (1998)
13. M. Hentschel, F. Guinea, Phys. Rev. B **76**, 115407 (2007)
14. A.H.C. Neto, V. Kotov, J. Nilsson, V. Pereira, N.M.R. Peres, B. Uchoa, Solid State Commun. **149**, 1094 (2009)
15. B. Uchoa, L. Yang, S.W. Tsai, N.M.R. Peres, A.H.C. Neto, Phys. Rev. Lett. **103**, 206804 (2009)
16. M. Vojta, L. Fritz, R. Bulla, Europhys. Lett. **90**, 27006 (2010)
17. K.H. Ding, A.G. Zhu, J. Berakdar, Phys. Rev. B **84**, 115433 (2011)
18. K. Saha, I. Paul, K. Sengupta, Phys. Rev. B **81**, 165446 (2010)
19. S.P. Chao, V. Aji, Phys. Rev. B **83**, 165449 (2011)
20. M. Kharitonov, G. Kotliar, Phys. Rev. B **88**, 201103 (2013)
21. A.K. Mitchell, M. Vojta, R. Bulla, L. Fritz, Phys. Rev. B **88**, 195119 (2013)
22. L. Fritz, M. Vojta, Rep. Prog. Phys. **76**, 032501 (2013)
23. Y.V. Nazarov, Y.M. Blanter, *Quantum Transport* (Cambridge University Press, Cambridge, 2009)
24. N.A. Zimbovskaya, M.R. Pederson, Phys. Rep. **509**, 1 (2011)
25. W. Liang, M. Bockrath, H. Park, Phys. Rev. Lett. **88**, 126801 (2002)
26. A.A. Balandin, Nat. Mater. **10**, 569 (2011)
27. Y.M. Zuev, W. Chang, P. Kim, Phys. Rev. Lett. **102**, 096807 (2009)
28. P. Wei, W. Bao, Y. Pu, C.N. Lau, J. Shi, Phys. Rev. Lett. **102**, 166808 (2009)
29. M.I. Alomar, D. Sánchez, Phys. Rev. B **89**, 115422 (2014)
30. M. Inglot, V.K. Dugaev, J. Barnaś, Phys. Rev. B **92**, 085418 (2015)
31. Y. Dubi, M.D. Ventra, Rev. Mod. Phys. **83**, 131 (2011)
32. D. Sánchez, H. Linke, New J. Phys. **16**, 110201 (2014)
33. D. Zubarev, Usp. Fiz. Nauk. **71**, 71 (1960)
34. C. Lacroix, J. Phys. F **11**, 2389 (1981)
35. Y. Meir, N.S. Wingreen, P.A. Lee, Phys. Rev. Lett. **70**, 2601 (1993)
36. V. Kashcheyevs, A. Aharony, O. Entin-Wohlman, Phys. Rev. B **73**, 125338 (2006)

37. T. Aono, J. Phys. Soc. Jpn. **82**, 083703 (2013)
38. Z.-G. Zhu, K.-H. Ding, J. Berakdar, Europhys. Lett. **90**, 67001 (2010)
39. L. Onsager, Phys. Rev. **37**, 405 (1931)
40. G.D. Mahan, *Many-Particle Physics*, 3rd edn. (Springer, NY, 2007)
41. P.N. Butcher, J. Phys.: Condens. Matter **2**, 4869 (1990)
42. J. Matthews, D. Sánchez, M. Larsson, H. Linke, Phys. Rev. B **85**, 205309 (2012)
43. H. Sevincli, C. Sevik, T. Cağin, G. Cuniberti, Sci. Rep. **3**, 035405 (2011)
44. B. Kubala, J. König, J. Pekola, Phys. Rev. Lett. **100**, 066801 (2008)
45. M. Eich, F. Herman, R. Pisoni, H. Overweg, Y. Lee, P. Rickhaus, K. Watanabe, T. Taniguchi, M. Sigrist, T. Ihn, K. Ensslin, Phys. Rev. X **8**, 031023 (2018)
46. D. Sánchez, R. López, C.R. Physique **17**, 1060 (2016)